

# Multiple Regulated Assembly, Crystal Structures and Magnetic Properties of Porous Coordination Polymers with Flexible Ligands

Chang-Yan Sun,<sup>[a]</sup> Xiang-Jun Zheng,<sup>[a]</sup> Song Gao,<sup>[bl]</sup> Li-Cun Li,<sup>[cl]</sup> and Lin-Pei Jin\*<sup>[al]</sup>

**Keywords:** Cobalt / Coordination polymers / Magnetic properties / Nickel / Porous materials

Four novel coordination polymers of Ni<sup>II</sup> and Co<sup>II</sup> with flexible ligands, namely [Ni(oba)(bpe)]<sub>n</sub>·nH<sub>2</sub>O (**1**), [Co(oba)(bpe)]<sub>n</sub> (**2**), [Ni<sub>2</sub>(oba)<sub>2</sub>(bpy)<sub>2</sub>(H<sub>2</sub>O)<sub>2</sub>]<sub>n</sub>·nbpy (**3**), and [Co(oba)(bpy)<sub>1/2</sub>]<sub>n</sub> (**4**) [H<sub>2</sub>oba = 4,4'-oxybis(benzoic acid), bpe = 1,2-bis(4-pyridyl)ethane, bpy = 4,4'-bipyridine] were synthesised by hydrothermal reactions and characterised by single-crystal X-ray diffraction, elemental analysis and IR spectroscopy. The Ni<sup>II</sup> ions in complex **1** are linked by flexible oba and bpe ligands to form square-grid-like corrugated sheets. These sheets are interpenetrated with each other, resulting in the formation of a 3D porous network with lattice water molecules in the channels. The variable temperature X-ray diffraction analysis shows that the framework is stable up to 300 °C despite the complete removal of the lattice water molecules during the heat treatment. Complex **2** can be re-

garded as possessing a  $\alpha$ -polonium-related topology. Triple interpenetration occurs to form a nonporous structure. In complex **3**, the oba and bpy ligands link Ni<sup>II</sup> ions into 1D train-like boxes. These boxes are entangled, with the aid of hydrogen bonds, leading to the formation of a 3D porous supramolecular architecture. Free bpy ligands reside in the channels. The Co<sup>II</sup> ions in complex **4** are linked by oba and bpy ligands to form a complicated 3D coordination polymer. The lattice water molecules in complex **1** and free bpy ligands in complex **3** can be regarded as templates that play an important role in the formation of the porous structures of complexes **1** and **3**. The magnetic properties of complexes **1**, **2**, and **4** have also been investigated.

(© Wiley-VCH Verlag GmbH & Co. KGaA, 69451 Weinheim, Germany, 2005)

## Introduction

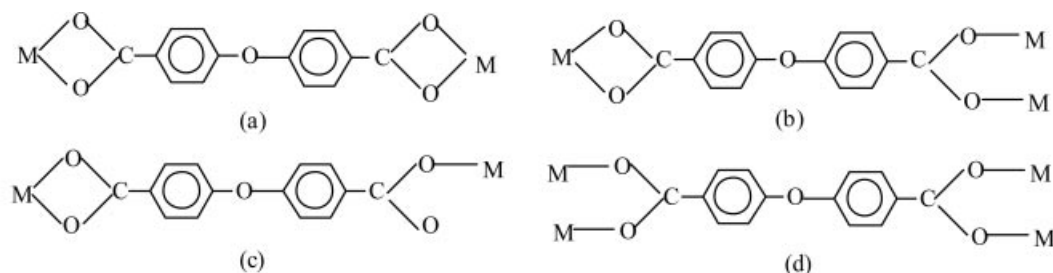
Porous coordination polymers are of current interest in the fields of supramolecular chemistry and crystal engineering not only because of the intriguing variety of architectures and topologies but also because of their potential applications in gas storage,<sup>[1]</sup> separation,<sup>[2]</sup> sensors<sup>[3]</sup> and catalysis.<sup>[4]</sup> The most commonly used synthetic strategy is to select appropriate ligands to bridge metal ions, with the aid of hydrogen bonds, metal–metal bonds,  $\pi$ - $\pi$  stacking, van der Waals and electrostatic interactions, to form the desired extended network under mild conditions.<sup>[5]</sup> It is well-known that the topology of porous coordination polymers depends both on the coordination behaviour of the organic ligands and on the selection of the coordination geometry of the metal centres. Thus far, porous coordination polymers have centred on the assembly of linear rigid polycarboxylates, especially dicarboxylates,<sup>[6,7]</sup> and d-block metal ions, as these metal ions have low coordination numbers and are

easily linked to form grid,<sup>[8]</sup> honeycomb,<sup>[9]</sup> brick-wall<sup>[10]</sup> and other geometries.<sup>[11]</sup> Long flexible ligands, because of their easy interpenetration, are seldom used in the construction of porous coordination polymers, although with ingenious design, interpenetrated networks can give novel topologies and useful properties.<sup>[12]</sup> More and more interest has focused on long flexible ligands recently, and how to avoid, or make use of, their interpenetration to construct porous coordination polymers is an interesting challenge. 4,4'-Oxybis(benzoic acid) (H<sub>2</sub>oba) is the typical example of a long, V-shaped, flexible ligand. As far as we know, its coordination chemistry has been studied and several coordination polymers have been obtained.<sup>[13]</sup> Of these coordination polymers, only one complex, [Zn<sub>2</sub>(oba)<sub>2</sub>(DMF)<sub>2</sub>]·2DMF, possesses a porous structure.<sup>[13f]</sup> In this complex, the DMF molecules act as guests, thus preventing interpenetrating. It is supposed that appropriate molecules may function as guests occupying the pores and consequently promote the formation of large pores,<sup>[14]</sup> and the introduction of ancillary ligands, such as the N-containing ligands 1,2-bis(4-pyridyl)ethane (bpe) and 4,4'-bipyridine (bpy), often has a significant effect on the formation and dimension of the resulting structures. With this idea in mind, we chose H<sub>2</sub>oba as a bridging ligand to react with the d-block metal ions Ni<sup>II</sup> and Co<sup>II</sup>. The neutral ligands bpe and bpy were introduced into the M<sup>II</sup>/oba system, and four novel coordination polymers, namely [Ni(oba)(bpe)]<sub>n</sub>·nH<sub>2</sub>O (**1**),

[a] Department of Chemistry, Beijing Normal University, Beijing 100875, China  
Fax: +86-10-5880-2075  
E-mail: lpjin@bnu.edu.cn

[b] State Key Laboratory of Rare Earth Materials Chemistry and Applications, College of Chemistry and Molecular Engineering, Peking University, Beijing, 100871, China

[c] Department of Chemistry, Nankai University, Tianjin 300071, China



Scheme 1. The coordination modes of the oba ligands in complexes 1–4.

[Co(oba)(bpe)]<sub>n</sub> (**2**), [Ni<sub>2</sub>(oba)<sub>2</sub>(bpy)<sub>2</sub>(H<sub>2</sub>O)<sub>2</sub>]<sub>n</sub>·nbpy (**3**) and [Co(oba)(bpy)<sub>1/2</sub>]<sub>n</sub> (**4**) were obtained. The details of their synthesis, structure and magnetic properties are reported below.

## Results and Discussion

### Description of the Structures

The oba ligands in complexes 1–4 are completely deprotonated and are significantly bent at the ether-oxygen sites [C–O–C = 115.9(3)–119.2(7)°]. They afford four kinds of coordination modes (see Scheme 1). All bpe ligands are in an *anti* conformation.

#### [Ni(oba)(bpe)]<sub>n</sub>·nH<sub>2</sub>O (**1**)

In the asymmetrical unit of complex **1**, there is one Ni<sup>II</sup> ion, one oba ligand, one bpe ligand and one lattice water molecule. The Ni<sup>II</sup> ion is located in a slightly distorted octahedral geometry and is coordinated to four oxygen atoms

of two oba ligands and two nitrogen atoms of two bpe ligands, as shown in Figure 1. The average Ni–N bond length is 2.051 Å and the Ni–O bond lengths are in the range 2.010(2)–2.312(3) Å. The details are depicted in Table 1. Each oba ligand adopts a bis(chelating bidentate) mode, linking two Ni<sup>II</sup> ions [see Scheme 1 (a)].

The Ni<sup>II</sup> ions are linked by oba and bpe ligands into square-grid-like corrugated sheets with grid dimensions of about 13 × 13 Å<sup>2</sup> in the *bc* plane, as shown in Figure 2 (a) (based on the separation of the metal ions). It is noteworthy that all the metal ions in the layer of complex **1** are not coplanar, but are present in a stair-like fashion. These stair-like layers are interpenetrated with each other, resulting in the formation of the 3D network. Although interpenetration occurs in complex **1**, there are still channels in the 3D network [see Figure 2 (b)], and lattice water molecules are accommodated in the channels. Hydrogen bonds are formed between the lattice water molecules and the carboxylate groups {*d*[O(6)⋯O(2)*i*] = 3.005 Å (symmetry code *i*: *x* + 1, *y*, *z*), *d*[O(2)*i*⋯H(6B)] = 2.562 Å and *θ*[O(6)–H(6B)]

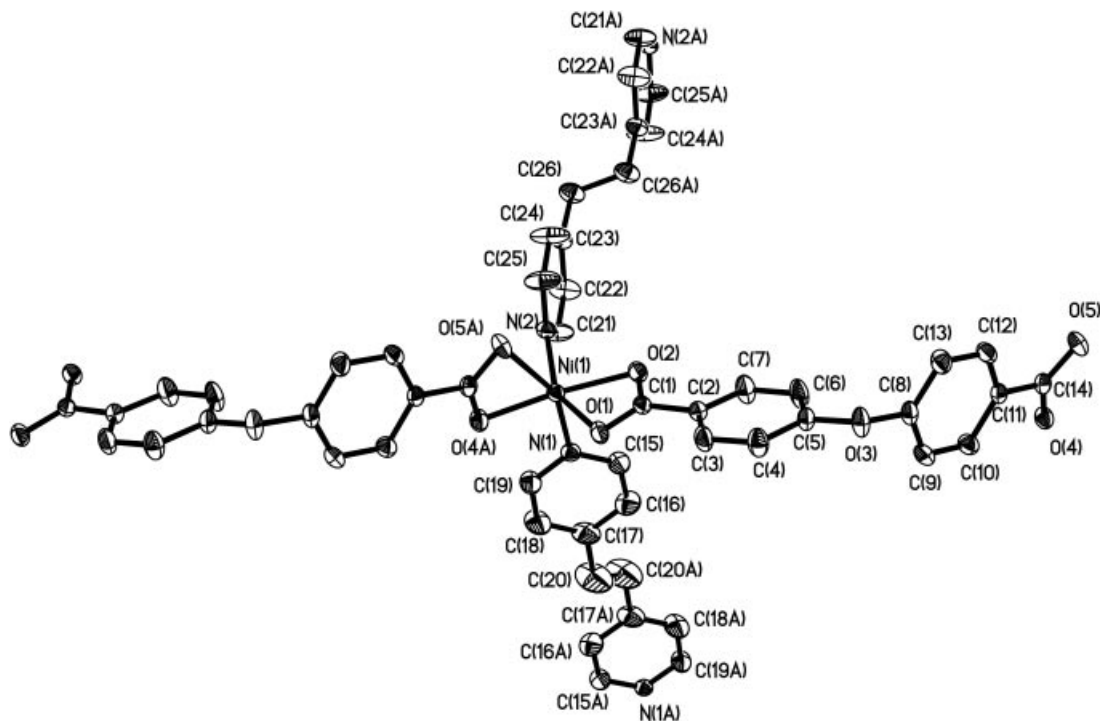


Figure 1. The coordination environment of the Ni<sup>II</sup> ion in complex **1** with 30% thermal ellipsoids. All hydrogen atoms and lattice water molecules have been omitted for clarity.

Table 1. Selected bond lengths [Å] and angles [°] for **1** and **2**.

<b>1</b> <sup>[a]</sup>			
Ni(1)–O(1)	2.169(3)	Ni(1)–O(5)#1	2.312(3)
Ni(1)–O(2)	2.073(2)	Ni(1)–N(1)	2.050(3)
Ni(1)–O(4)#1	2.010(2)	Ni(1)–N(2)	2.053(3)
O(1)–Ni(1)–O(5)#1	86.89(9)	N(1)–Ni(1)–O(1)	96.67(1)
O(2)–Ni(1)–O(1)	61.79(9)	N(1)–Ni(1)–O(2)	96.14(1)
O(2)–Ni(1)–O(5)#1	107.86(9)	N(1)–Ni(1)–O(5)#1	154.26(1)
O(4)#1–Ni(1)–O(1)	97.82(1)	N(1)–Ni(1)–N(2)	98.24(1)
O(4)#1–Ni(1)–O(2)	158.11(1)	N(2)–Ni(1)–O(1)	150.66(1)
O(4)#1–Ni(1)–O(5)#1	60.22(9)	N(2)–Ni(1)–O(2)	91.53(1)
O(4)#1–Ni(1)–N(1)	94.05(1)	N(2)–Ni(1)–O(5)#1	90.47(1)
O(4)#1–Ni(1)–N(2)	106.13(1)		
<b>2</b> <sup>[b]</sup>			
Co(1)–O(1)	2.020(2)	Co(1)–O(5)#3	2.232(2)
Co(1)–O(2)#1	2.026(2)	Co(1)–N(1)	2.164(3)
Co(1)–O(4)#3	2.170(2)	Co(1)–N(2)#2	2.147(3)
O(1)–Co(1)–O(2)#1	112.46(8)	O(2)#1–Co(1)–N(1)	90.17(8)
O(1)–Co(1)–O(4)#3	151.03(8)	O(2)#1–Co(1)–N(2)#2	89.76(8)
O(1)–Co(1)–O(5)#3	91.35(9)	N(1)–Co(1)–O(4)#3	87.64(9)
O(1)–Co(1)–N(1)	87.89(9)	N(2)#2–Co(1)–O(4)#3	88.73(9)
O(1)–Co(1)–N(2)#2	95.52(9)	N(2)#2–Co(1)–N(1)	176.34(8)
O(2)#1–Co(1)–O(4)#3	96.17(8)		

[a] Symmetry transformations used to generate equivalent atoms: #1  $x, y - 1, z + 1$ . [b] Symmetry transformations used to generate equivalent atoms: #1  $-x + 1, -y, -z + 1$ ; #2  $x + 1, y, z + 1$ ; #3  $x + 1, -y + 1/2, z - 1/2$ .

$\cdots\text{O}(2)\text{i}] = 111.69^\circ$ }, which enhances the stability of the open framework.

### [Co(oba)(bpe)]<sub>n</sub> (**2**)

In complex **2**, one carboxylate group of an oba ligand adopts a chelating bidentate mode while the other adopts a bridging bidentate mode, which means that every oba ligand links three Co<sup>II</sup> ions [see Scheme 1 (b)]. There is only one crystallographically unique Co<sup>II</sup> centre, which is coordinated to four carboxylate oxygen atoms of three oba ligands and two nitrogen atoms of two bpe ligands (see Figure 3). The average Co–N bond length is 2.155 Å and the Co–O bond lengths are in the range 2.020(2)–2.232(2) Å. Thus, the Co<sup>II</sup> centre displays a distorted octahedral geometry with one [CoO<sub>4</sub>N<sub>2</sub>] unit. Two such [CoO<sub>4</sub>N<sub>2</sub>] units are connected together by two carboxylate groups, leading to the formation of a binuclear secondary building unit (SBU) in which the Co $\cdots$ Co distance is 4.298 Å. The oba ligands link the SBUs into 2D layers with rhombus-shaped cavities of about  $13 \times 15 \text{ \AA}^2$ . Although this framework motif is common, the bent oba structure provides a new aspect in the cavity shape, and it has seldom been reported that this motif contains concertinaed corners.<sup>[15]</sup> These layers are pillared by bpe ligands with a Co–N coordination bond, resulting in the formation of a 3D net that can be regarded as possessing an  $\alpha$ -polonium-related topology [see Figure 4 (a)]. There are large channels ( $13 \times 15 \text{ \AA}^2$ ) in the open sub-framework (named net), but triple interpenetration occurs, as shown in Figure 4 (b). The nodes of the second and third nets are located, equally spaced, along the rhombohedral diagonal of the first net, and each rhombic “window” has

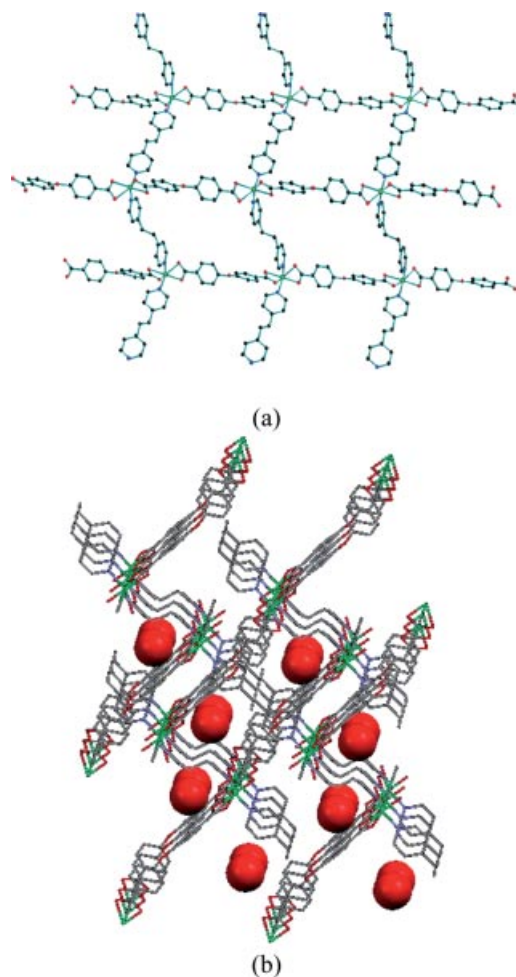


Figure 2. (a) Square-grid-like sheet of complex **1** in the *bc* plane. (b) The 3D porous network of complex **1**, with lattice water molecules in the channels, viewed along the *a* axis.

a rod from each of the adjacent two nets passing through it, giving a complicated nonporous structure.

### [Ni<sub>2</sub>(oba)<sub>2</sub>(bpy)<sub>2</sub>(H<sub>2</sub>O)<sub>2</sub>]<sub>n</sub>·nbpv (**3**)

There are two kinds of metal coordination environments in complex **3**, as shown in Figure 5. Ni(1) and Ni(2) are both six-coordinate and their coordination geometries can be described as distorted octahedral. Both Ni<sup>II</sup> ions are coordinated to three oxygen atoms of two oba ligands, two nitrogen atoms of two bpy ligands and one oxygen atom of one water molecule. However, the corresponding bond lengths and bond angles are different. The Ni(1)–O bond lengths are in the range 1.992(4)–2.143(5) Å and the average value is 2.095 Å, while for Ni(2) the bond lengths range from 2.026(4) Å to 2.195(4) Å and the average value is 2.091 Å. The details are depicted in Table 2. In complex **3**, one carboxylate group of an oba ligand coordinates to a Ni<sup>II</sup> ion in a monodentate mode while the other adopts a chelating-bidentate mode. Thus, every oba ligand links two Ni<sup>II</sup> ions [see Scheme 1 (c)]. Ni(1) and Ni(2) are bridged by a bpy ligand with a distance of 11.129 Å, which can be regarded as a binuclear SBU. Such SBUs are linked together

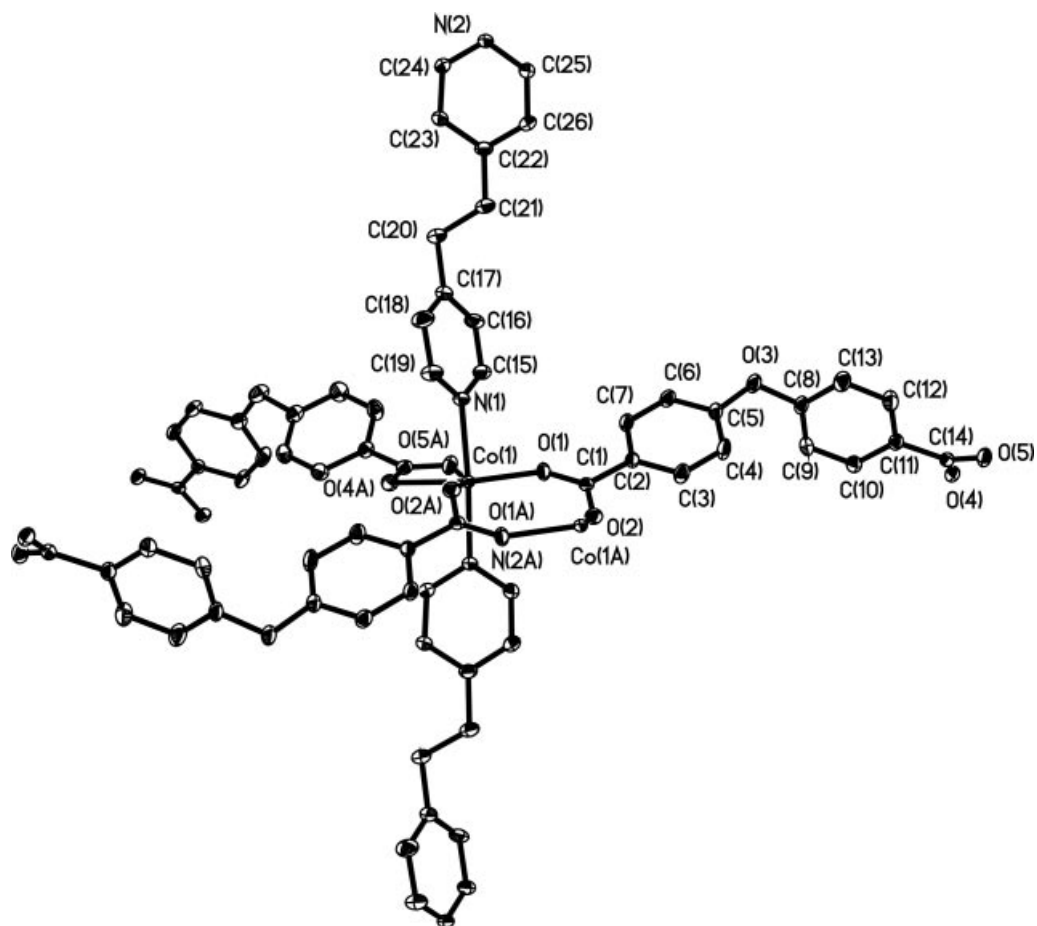


Figure 3. The coordination environment of the  $\text{Co}^{\text{II}}$  ion in complex **2** with 30% thermal ellipsoids. All hydrogen atoms have been omitted for clarity.

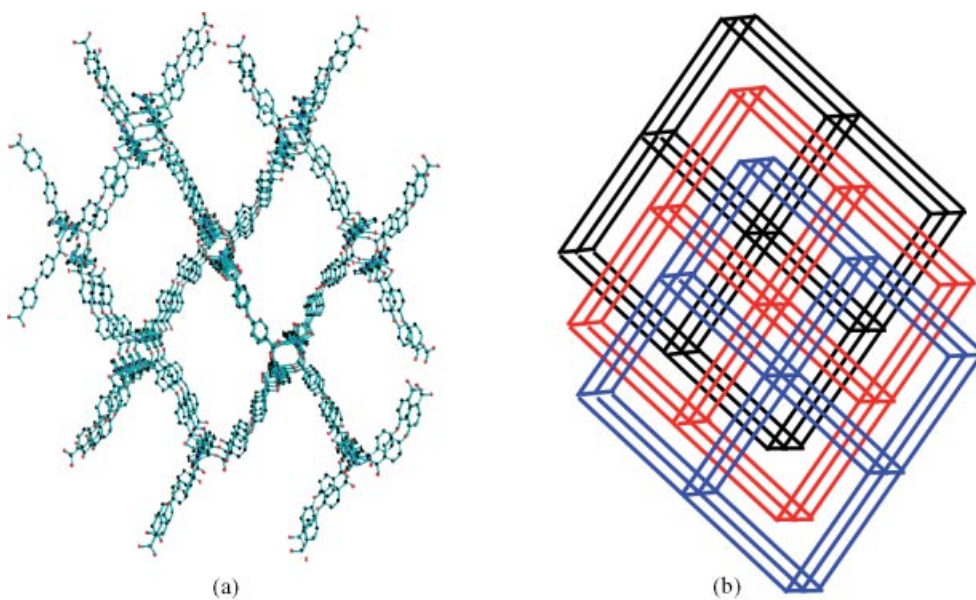


Figure 4. (a) The 3D framework of complex **2** with channels viewed along the [101] direction. (b) A simplified representation of the interpenetrating framework of complex **2**, the alternating frameworks are shown in black, red and blue.

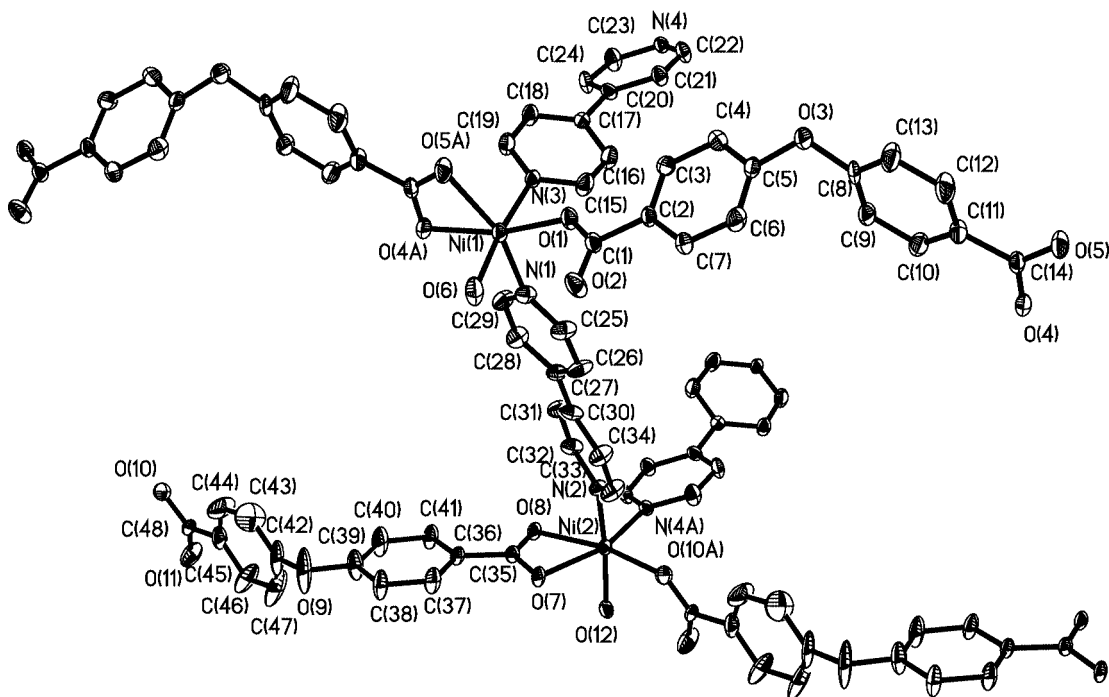


Figure 5. The coordination environments of the Ni<sup>II</sup> ions in complex **3** with 30% thermal ellipsoids. All hydrogen atoms and free bpy ligands have been omitted for clarity.

Table 2. Selected bond lengths [Å] and angles [°] for **3** and **4**.

3 <sup>[a]</sup>			
Ni(1)–O(1)	1.992(4)	Ni(2)–O(7)	2.195(4)
Ni(1)–O(4)#1	2.054(4)	Ni(2)–O(8)	2.112(4)
Ni(1)–O(5)#1	2.143(5)	Ni(2)–O(10)#2	2.026(4)
Ni(1)–O(6)	2.081(5)	Ni(2)–O(12)	2.030(4)
Ni(1)–N(1)	2.053(6)	Ni(2)–N(2)	2.060(5)
Ni(1)–N(3)	2.137(5)	Ni(2)–N(4)#3	2.059(5)
O(1)–Ni(1)–O(4)#1	165.4(2)	O(8)–Ni(2)–O(7)	60.77(2)
O(1)–Ni(1)–O(5)#1	103.88(2)	O(10)#2–Ni(2)–O(7)	103.92(2)
O(1)–Ni(1)–O(6)	90.76(2)	O(10)#2–Ni(2)–O(8)	164.60(2)
O(1)–Ni(1)–N(3)	85.10(2)	O(10)#2–Ni(2)–O(12)	88.67(2)
O(4)#1–Ni(1)–O(5)#1	61.81(2)	O(10)#2–Ni(2)–N(2)	90.83(2)
O(4)#1–Ni(1)–O(6)	92.89(2)	O(10)#2–Ni(2)–N(4)#3	96.43(2)
O(4)#1–Ni(1)–N(3)	92.18(2)	O(12)–Ni(2)–O(7)	88.91(2)
O(6)–Ni(1)–O(5)#1	93.5(2)	O(12)–Ni(2)–O(8)	89.29(2)
O(6)–Ni(1)–N(3)	174.03(2)	O(12)–Ni(2)–N(2)	172.71(2)
N(1)–Ni(1)–O(4)#1	94.8(2)	O(12)–Ni(2)–N(4)#3	93.75(2)
N(1)–Ni(1)–O(5)#1	156.5(2)	N(2)–Ni(2)–O(7)	84.15(2)
N(1)–Ni(1)–O(6)	89.1(2)	N(2)–Ni(2)–O(8)	89.27(2)
N(1)–Ni(1)–N(3)	87.3(2)	N(4)#3–Ni(2)–O(7)	159.54(2)
		N(4)#3–Ni(2)–O(8)	98.94(2)
		N(4)#3–Ni(2)–N(2)	93.5(2)
4 <sup>[b]</sup>			
Co(1)–O(1)	2.077(3)	Co(1)–O(5)#1	1.976(3)
Co(1)–O(2)#2	2.000(3)	Co(1)–N(1)	2.084(3)
Co(1)–O(4)#3	2.020(3)		
O(1)–Co(1)–N(1)	170.89(2)	O(4)#3–Co(1)–N(1)	88.85(2)
O(2)#2–Co(1)–O(1)	85.31(1)	O(5)#1–Co(1)–O(1)	88.94(1)
O(2)#2–Co(1)–O(4)#3	141.82(2)	O(5)#1–Co(1)–O(2)#2	112.92(2)
O(2)#2–Co(1)–N(1)	87.87(1)	O(5)#1–Co(1)–O(4)#3	104.97(1)
O(4)#3–Co(1)–O(1)	100.25(1)	O(5)#1–Co(1)–N(1)	88.15(1)

[a] Symmetry transformations used to generate equivalent atoms: #1  $x, y + 1, z$ ; #2  $x, y - 1, z$ ; #3  $-x + 1, -y + 1, -z + 2$ . [b] Symmetry transformations used to generate equivalent atoms: #1  $-x + 2, -y + 1, -z + 2$ ; #2  $-x + 2, y, -z + 3/2$ ; #3  $x, y - 1, z$ .

by the oba ligands, resulting in 1D train-like boxes that contain free bpy ligands (see Figure 6). Each box is entangled with another two adjacent boxes. There are hydrogen bonds between the water molecules and the carboxylate groups  $\{d[\text{O}(6)\cdots\text{O}(2)] = 2.669 \text{ \AA}$ ,  $d[\text{O}(2)\cdots\text{H}(6\text{A})] = 2.128 \text{ \AA}$  and  $\theta[\text{O}(6)\text{---}\text{H}(6\text{A})\cdots\text{O}(2)] = 113.19^\circ$ ;  $d[\text{O}(12)\cdots\text{O}(11)\text{i}] = 2.553 \text{ \AA}$  (symmetry code  $i: x, y - 1, z$ ),  $d[\text{O}(11)\cdots\text{H}(12\text{B})] = 2.027 \text{ \AA}$  and  $\theta[\text{O}(12)\text{---}\text{H}(12\text{B})\cdots\text{O}(11)\text{i}] = 119.37^\circ\}$ , which leads to the formation of a 3D porous supramolecular architecture.

#### The Structure of $[\text{Co}(\text{oba})(\text{bpy})_{1/2}]_n$ (**4**)

The coordination environment of the Co<sup>II</sup> ions in complex **4** is shown in Figure 7. The Co<sup>II</sup> ion is five-coordinate, with four oxygen atoms from four oba ligands and one nitrogen atom from one bpy ligand. The coordination geometry of the Co<sup>II</sup> ion can best be described as a distorted trigonal bipyramid. The Co–N bond length is 2.084(3) Å and the Co–O bond lengths are in the range 1.976(3)–2.077(3) Å. Every oba ligand in complex **4** adopts a bis(bridging-bidentate) mode and links four Co<sup>II</sup> ions [see Scheme 1 (d)]. The Co<sup>II</sup> ions are bridged by the carboxylate groups of oba ligands into 1D chains along the  $c$  axis, in which the adjacent Co<sup>II</sup>–Co<sup>II</sup> distances are alternately 3.288 Å and 4.238 Å. These chains are further bridged by the bent oba ligands to produce 2D regular metal-organic layers. When viewed along the  $c$  axis, these 2D layers can be regarded as sine- and cosine-type curves intersecting at the zero points. The bpy ligands connect the Co<sup>II</sup> ions in these 2D layers into a 3D structure.

#### Effect of the Metal Ions on the Molecular Structure

It is interesting that, although they are bound to the same ligands, Ni<sup>II</sup> and Co<sup>II</sup> give completely different pro-

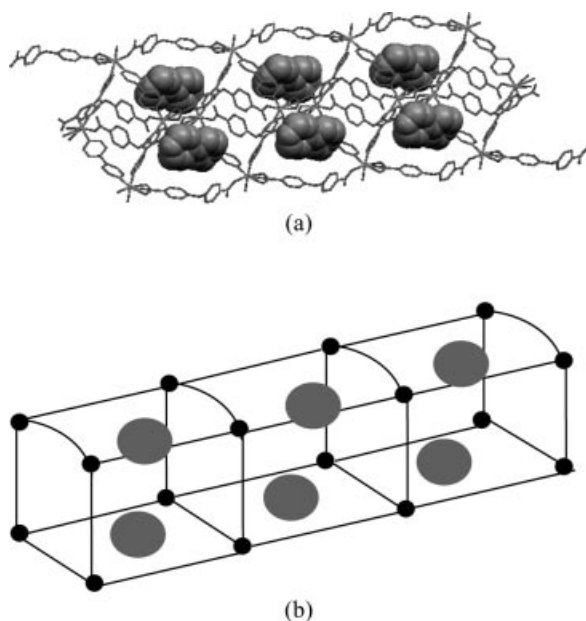


Figure 6. (a) The 1D train-like box in complex **3** (space-filling diagrams represent free bpy ligands). (b) A simplified representation of the 1D train-like box in complex **3** (nodes represent Ni<sup>II</sup> ions and the balls represent free bpy ligands).

ducts, as shown in Scheme 2. We found from the structural analysis of complexes **1–4** that the two Ni<sup>II</sup> complexes **1** and **3** possess a 3D open supramolecular architecture while the two Co<sup>II</sup> complexes **2** and **4** have a 3D non-porous structure. Taking **1** and **2** as examples, the Ni<sup>II</sup> and Co<sup>II</sup> ions are both six-coordinate and in distorted octahedral geometries, but their coordination environments are different. In complex **1**, there are two oba ligands and two bpe ligands around each Ni<sup>II</sup> ion, while in complex **2**, there are three oba ligands and two bpe ligands around each Co<sup>II</sup> ion. More ligands are around each Co<sup>II</sup> ion than each Ni<sup>II</sup> ion. This is consistent with the fact that the radius of Co<sup>II</sup> ion is larger than that of Ni<sup>II</sup> ion. Furthermore, the coordination modes of the oba ligands in the two complexes are

different. The oba ligands adopt a bis(chelating-bidentate) mode in complex **1** and a chelating-bridging mode in complex **2** (see parts a and b in Scheme 1), which results in the different structures of the corresponding complexes. Similar results are found for complexes **3** and **4**. This may also be attributed to the different size of the metal ions. Lower-dimensional nets are usually less likely to interpenetrate because there are more possible ways to maximize the packing efficiency.<sup>[16]</sup> So, after the stacking of 2D layers, complex **1** possesses 3D porous structure, while triple interpenetration occurs in complex **2**, as shown in Figure 6, to give a non-porous structure. A rational assembly of metal ions and flexible ligands is critical for the formation of a porous structure.

### Effect of the Ligand on the Molecular Structure

Although the bpe and bpy ligands are both N-containing spacers, they are quite different. For example, bpe has *anti* and *gauche* conformations and is more flexible than bpy. When the bpe ligand is in the *anti* conformation, the distance between the two nitrogen atoms is larger than that of the bpy ligand, therefore *anti*-bpe is a longer spacer than bpy. When the bpe ligand is introduced into the M<sup>II</sup>/H<sub>2</sub>oba system, we obtain 2D square-grid-like sheets for Ni<sup>II</sup> and a 3D  $\alpha$ -polonium-related framework for Co<sup>II</sup>, while with bpy we obtain 1D train-like boxes for the Ni<sup>II</sup> complex and a complicated 3D framework for the Co<sup>II</sup> complex. The oba ligands in the four complexes adopt four different coordination modes, as shown in Scheme 1, so for a special M<sup>II</sup>/H<sub>2</sub>oba system, the ancillary ligand has a significant effect on the formation and structure of the coordination polymers. In order to construct porous coordination polymers, it is a feasible method to introduce ancillary ligands.

### Effect of Guest Molecules on the Molecular Structure

From the structural descriptions above, we know that lattice water molecules are accommodated in the channels of

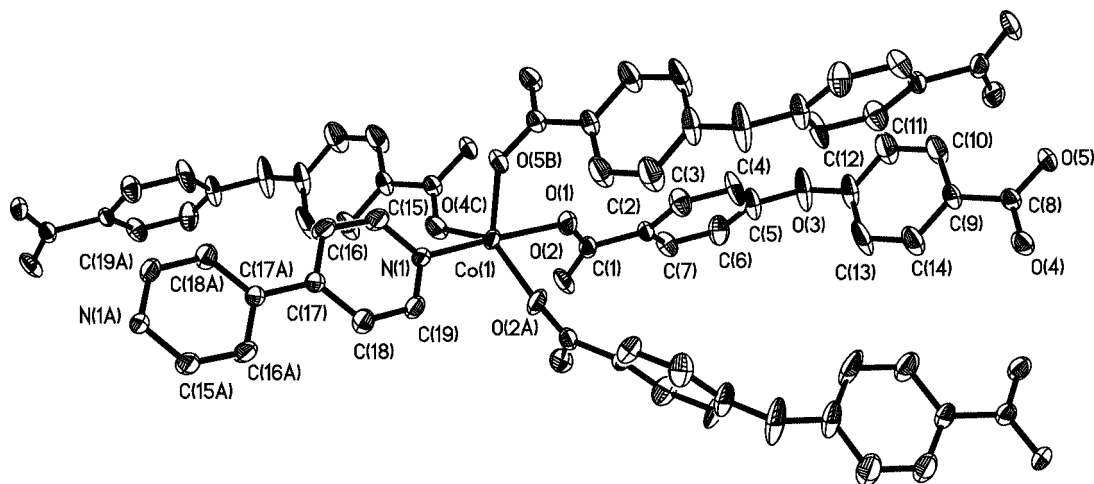
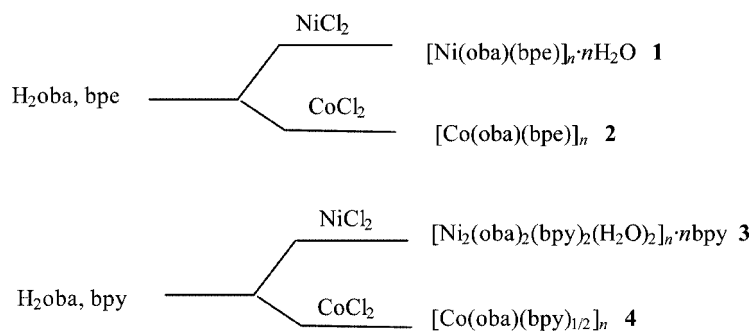


Figure 7. The coordination environment of the Co<sup>II</sup> ion in complex **4** with 30% thermal ellipsoids. All hydrogen atoms have been omitted for clarity.



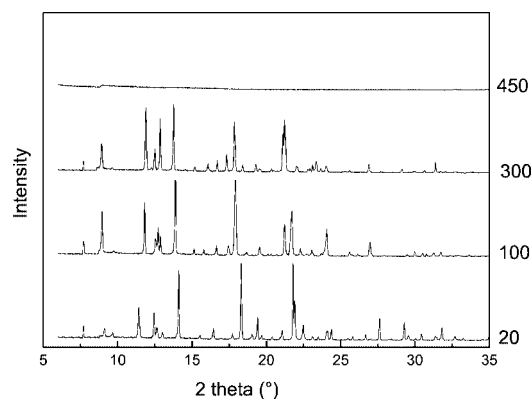
Scheme 2. Self-assembly of the coordination polymers.

complex **1** and free bpy ligands reside in the channels of complex **3**. The presence of lattice water molecules and free bpy ligands may be one of the more important factors for constructing the porous structures of complexes **1** and **3** as they occupy the pores and function as templates, thus preventing further interpenetration. This provides a valuable approach for constructing porous coordination polymers. If the potential pore walls are formed by the hydrophobic parts of ligand molecules, we can introduce hydrophobic molecules to function as guest molecules and occupy the pores through hydrophobic interactions with the ligands;<sup>[2b,14]</sup> on the other hand, if the potential pore walls are formed by the hydrophilic parts of ligand molecules, we can introduce hydrophilic molecules.<sup>[17]</sup> It can be expected that the presence of these guest molecules promotes the formation of large pores.

### Thermal Stability Analysis of Complex 1

The thermal analysis of complex **1** is consistent with the crystallographic observations. The TG curve shows that the first weight loss of 3.7% from 75 °C to 290 °C corresponds to the loss of the lattice water molecules (calcd. 3.5%), leaving a framework of [Ni(oba)(bpe)]. This framework remains stable beyond 300 °C and it begins to decompose at 390 °C. This further decomposition finishes at 550 °C, leaving a powder of NiO. It is the interpenetrated nature of the structure that causes the higher thermal stability of complex **1**.

To further test the thermal stability of complex **1**, powder samples were examined by powder X-ray diffraction analysis. Corresponding to the TG analysis, powder XRD patterns were recorded at 20, 100, 300 and 450 °C (see Figure 8). It can be seen from Figure 8 that the XRD patterns at 100 °C and 300 °C are similar to that at room temperature, but not the same, indicating that the framework is able to survive. However, there are changes in the XRD patterns at 20, 100, and 300 °C, which are probably due to the contraction of the structure upon removal of the water molecules and the presence of the flexible ligands. At 450 °C, the XRD pattern changes completely, revealing the collapse of the framework, which is in accordance with the result of the thermogravimetric analysis.

Figure 8. The powder X-ray diffraction patterns of complex **1** at different temperatures.

### Magnetic Properties

Because the bridging ligands oba, bpe and bpy are quite long in complexes **1** and **3**, and thus the Ni $\cdots$ Ni distances are very long too, the magnetic interactions transferred by these ligands should be very weak. The magnetic properties of complexes **1** and **3** can be regarded as those of a single metal ion anisotropy. Here, we only give the magnetic property of complex **1** as an example.

#### Complex 1

The magnetic properties of complex **1** in the form of  $\chi_M$  and  $\mu_{\text{eff}}$  vs.  $T$  plots ( $\chi_M$  is the molar magnetic susceptibility and  $\mu_{\text{eff}}$  is the effective magnetic moment) are shown in Figure 9. Data were collected in the range 2–300 K in a magnetic field of 5 kOe. The  $\mu_{\text{eff}}$  value for complex **1** is 3.15  $\mu_B$  at 300 K and it is practically constant in the temperature range analysed. It only starts to decrease at around 10 K, reaching a minimum value of 2.83  $\mu_B$  at 2 K, which should be mainly attributed to the zero-field splitting of Ni<sup>II</sup> ions.

The experimental susceptibility data were fitted to the equation that considers only non-interacting  $S = 1$  ions in the presence of a single ion anisotropy. The magnetic susceptibility is given in Equation (1).<sup>[18]</sup>

$$\chi_M = \frac{2Ng^2\beta^2}{3kT} \times \frac{2x^{-1} - 2\exp(-x)x^{-1} + \exp(-x)}{1 + 2\exp(-x)} \quad (1)$$

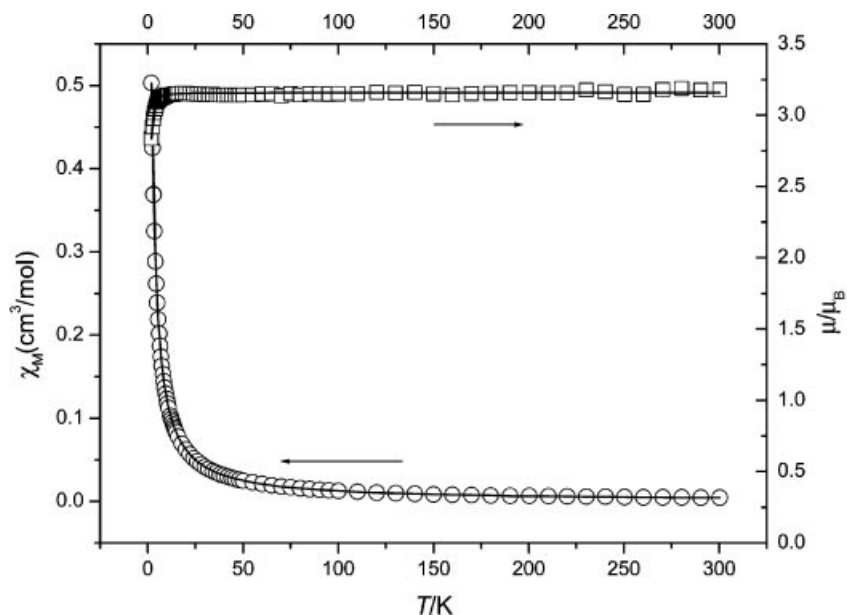


Figure 9. Plots of  $\chi_M$  (○) and  $\mu_{\text{eff}}$  (□) vs.  $T$  for complex 1; the solid lines are theoretical fits based on Equation (1).

where  $x = D/kT$ . The best fit is given by the parameters  $g = 2.23$ ,  $D = 2.62 \text{ cm}^{-1}$ , with an agreement factor,  $R$ , of  $2.03 \times 10^{-4}$   $\{R = \sum[(\chi_M)_{\text{obs}} - (\chi_M)_{\text{calc}}]^2 / \sum[(\chi_M)_{\text{calc}}]^2\}$ .

#### Complex 2

The magnetic susceptibility data of complex 2 in the form of  $1/\chi_M$  and  $\mu_{\text{eff}}$  vs.  $T$  plots are given in Figure 10. They were measured in the range 2–300 K in a magnetic field of 1 kOe. It can be seen that the  $\mu_{\text{eff}}$  value decreases very gradually upon cooling and the  $\mu_{\text{eff}}$  value at 300 K is  $4.25 \mu_B$ , which is larger than that expected for the spin-only case of  $\text{Co}^{\text{II}}$  ( $\mu_{\text{eff}} = 3.87 \mu_B$ ), indicating an unquenched orbital contribution. The magnetic data above 30 K can be fitted to the Curie–Weiss law with  $C = 2.268(5) \text{ cm}^3 \text{ mol}^{-1} \text{ K}$  and  $\theta = -1.8 \text{ K}$ . The  $C$  value corresponds to  $g = 2.20$  with  $S = 3/2$ . These results suggest a possible very weak antiferromagnetic coupling.

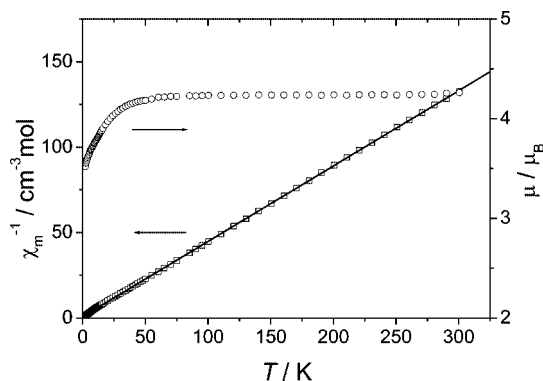


Figure 10. Plots of  $1/\chi_M$  (□) and  $\mu_{\text{eff}}$  (○) vs.  $T$  for complex 2; the solid line is the theoretical fit based on the Curie–Weiss law.

#### Complex 4

Figure 11 shows the magnetic properties of complex 4 in the form of  $1/\chi_M$  and  $\mu_{\text{eff}}$  vs.  $T$  plots in the range 2–300 K measured at 1 kOe. It can be seen that the  $\mu_{\text{eff}}$  value decreases very gradually upon cooling and the  $\mu_{\text{eff}}$  value at 300 K is  $4.71 \mu_B$ , which is obviously larger than the expected spin-only value of  $3.87 \mu_B$  for a  $\text{Co}^{\text{II}}$  ion with  $S = 3/2$ , thus showing an unquenched orbital contribution. The magnetic data above 50 K can be fitted to the Curie–Weiss law with  $C = 2.836(6) \text{ cm}^3 \text{ mol}^{-1} \text{ K}$  and  $\theta = -7.3(1) \text{ K}$ . The  $C$  value corresponds to  $g = 2.46$  with  $S = 3/2$ . These results suggest a weak antiferromagnetic interaction.

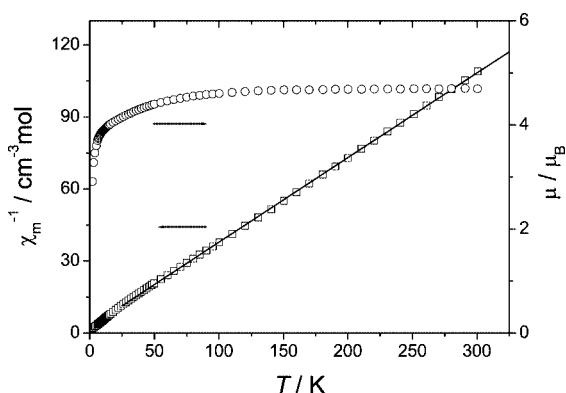


Figure 11. Plots of  $1/\chi_m$  (□) and  $\mu_{\text{eff}}$  (○) vs.  $T$  for complex 4; the solid line is the best fit based on the Curie–Weiss law.

## Conclusions

We have successfully obtained four novel coordination polymers of  $\text{Ni}^{\text{II}}$  and  $\text{Co}^{\text{II}}$ , namely  $[\text{Ni}(\text{oba})(\text{bpe})]_n \cdot n\text{H}_2\text{O}$

(1), [Co(oba)(bpe)]<sub>n</sub> (2), [Ni<sub>2</sub>(oba)<sub>2</sub>(bpy)<sub>2</sub>(H<sub>2</sub>O)<sub>2</sub>]<sub>n</sub>·*n*bpy (3) and [Co(oba)(bpy)<sub>1/2</sub>]<sub>n</sub> (4), with different dimensionalities. Comparing the structures of complexes 1 and 2, and complexes 3 and 4, it has been found that the different size of the metal ions has a significant effect on the formation and dimensions of the resulting structures. Furthermore, comparing the structures of complexes 1 and 3, and complexes 2 and 4, we can see that the neutral ancillary ligand is very important for the formation of coordination polymers. The presence of guest molecules can promote the formation of larger pores.

## Experimental Section

**General Remarks:** All reagents were used as received without further purification. The C, H and N microanalyses were carried out with a Vario EL elemental analyzer. The IR spectra were recorded with a Nicolet Avatar 360 FT-IR spectrometer using the KBr pellet technique. Thermogravimetric curves were measured on a Perkin-Elmer TGA-7 (USA) at a heating rate of 5 °C min<sup>-1</sup> from room temperature to 600 °C under nitrogen. The magnetic susceptibilities were obtained on crystalline samples using a Quantum Design MPMS SQUID magnetometer. The experimental susceptibilities were corrected for the sample holder and the diamagnetism contributions estimated from Pascal's constants. The powder X-ray diffraction patterns were recorded on a Bruker AXS D8 ADVANCE diffractometer.

**Synthesis of [Ni(oba)(bpe)]<sub>n</sub>·*n*H<sub>2</sub>O (1):** A mixture of H<sub>2</sub>oba (0.1 mmol), NiCl<sub>2</sub>·6H<sub>2</sub>O (0.1 mmol), bpe (0.1 mmol) and 5 mL of deionised water was placed in a Teflon-lined stainless vessel (25 mL) and 0.2 mL of a 0.65 M aqueous NaOH solution was added whilst stirring. The vessel was then sealed and heated to 180 °C for 72 h under autogenous pressure, and then cooled slowly to room temperature. Single crystals were obtained by filtration, washed with deionized water and ethanol, and dried in air. Yield: 0.042 g (81.2%) C<sub>26</sub>H<sub>22</sub>NiN<sub>2</sub>O<sub>6</sub> (517.17): calcd. C 60.33, H 4.25, N 5.41; found C 60.44, H 3.91, N 5.53. IR data (KBr pellet):  $\tilde{\nu}$  = 3449 cm<sup>-1</sup> (m), 3063 (w), 2929 (w), 1616 (m), 1596 (s), 1534 (m), 1504 (m), 1417 (s), 1226 (m), 1165 (m), 1098 (w), 1071 (w), 1025 (w), 876 (m), 835 (w), 781 (m), 662 (w), 548 (w).

**Synthesis of [Co(oba)(bpe)]<sub>n</sub> (2):** The synthesis of complex 2 followed the same procedure as complex 1 except that the volume of aqueous NaOH solution added was 0.3 mL. Yield: 0.04 g (80.1%) C<sub>26</sub>H<sub>20</sub>CoN<sub>2</sub>O<sub>5</sub> (499.37): calcd. C 62.48, H 4.00, N 5.61; found C 62.70, H 4.13, N 5.50. IR data (KBr pellet):  $\tilde{\nu}$  = 3445 cm<sup>-1</sup> (m), 3058 (w), 2971 (w), 2928 (w), 1616 (m), 1596 (s), 1538 (m), 1503 (m), 1417 (s), 1227 (s), 1163 (m), 1094 (w), 1049 (w), 1025 (w), 875 (m), 836 (w), 781 (m), 662 (w), 546 (w).

**Synthesis of [Ni<sub>2</sub>(oba)<sub>2</sub>(bpy)<sub>2</sub>(H<sub>2</sub>O)<sub>2</sub>]<sub>n</sub>·*n*bpy (3):** A mixture of H<sub>2</sub>oba (0.1 mmol), NiCl<sub>2</sub>·6H<sub>2</sub>O (0.1 mmol), bpy (0.1 mmol) and 5 mL of deionised water was placed in a Teflon-lined stainless vessel (25 mL) and 0.2 mL of a 0.65 M aqueous NaOH solution was added whilst stirring. The vessel was then sealed and heated to 180 °C for 72 h under autogenous pressure, and then cooled slowly to room temperature. Single crystals were obtained by filtration, washed with deionized water and ethanol, and dried in air. Yield: 0.024 g (42.3%) C<sub>58</sub>H<sub>44</sub>N<sub>6</sub>Ni<sub>2</sub>O<sub>12</sub> (1134.4): calcd. C 61.35, H 3.88, N 7.40; found C 61.20, H 3.74, N 7.04. IR data (KBr pellet):  $\tilde{\nu}$  = 3444 cm<sup>-1</sup> (m), 1595 (s), 1540 (m), 1496 (w), 1420 (s), 1381 (s), 1300 (w), 1248 (m), 1232 (m), 1158 (w), 875 (w), 808 (w), 784 (w), 659 (w), 635 (w).

**Synthesis of [Co(oba)(bpy)<sub>1/2</sub>]<sub>n</sub> (4):** The synthesis of complex 4 was similar to that of complex 3. Yield: 0.027 g (68.7%) C<sub>19</sub>H<sub>12</sub>CoNO<sub>5</sub> (393.23): calcd. C 57.98, H 3.05, N 3.56; found C 57.95, H 3.03, N 4.01. IR data (KBr pellet):  $\tilde{\nu}$  = 3436 cm<sup>-1</sup> (w), 3063 (w), 2924 (w), 1594 (s), 1551 (m), 1499 (m), 1393 (s), 1299 (w), 1240 (s), 1221 (m), 1159 (m), 1013 (w), 877 (m), 779 (m), 675 (w), 565 (w), 514 (w).

**X-ray Crystallographic Study:** Diffraction intensities for the four complexes were collected at 293 K on a Bruker SMART 1000 CCD diffractometer employing graphite-monochromated Mo-*K*<sub>α</sub> radiation ( $\lambda$  = 0.71073 Å). A semi-empirical absorption correction was applied using the SADABS program.<sup>[19]</sup> The structures were solved by direct methods and refined by full-matrix least-squares on *F*<sup>2</sup> using the SHELXS 97 and SHELXL 97 programs, respectively.<sup>[20,21]</sup> Non-hydrogen atoms were refined anisotropically and hydrogen atoms were placed in geometrically calculated positions. The crystallographic data for complexes 1–4 are listed in Table 3, and selected bond lengths and angles are listed in Tables 1 and 2. CCDC-265220–265223 (for 1–4, respectively) contain the supplementary crystallographic data for this paper. These data can be

Table 3. Crystal data and structure refinement parameters for 1–4.

	1	2	3	4
Chemical formula	C <sub>26</sub> H <sub>22</sub> N <sub>2</sub> NiO <sub>6</sub>	C <sub>26</sub> H <sub>20</sub> CoN <sub>2</sub> O <sub>5</sub>	C <sub>58</sub> H <sub>44</sub> N <sub>6</sub> Ni <sub>2</sub> O <sub>12</sub>	C <sub>19</sub> H <sub>12</sub> CoNO <sub>5</sub>
Crystal system	triclinic	monoclinic	triclinic	monoclinic
Space group	<i>P</i> $\bar{1}$	<i>P</i> 2 <sub>1</sub> / <i>c</i>	<i>P</i> $\bar{1}$	<i>C</i> 2/ <i>c</i>
Formula mass	517.17	499.37	1134.41	393.23
<i>a</i> [Å]	9.254(3)	10.466(6)	12.375(5)	22.376(7)
<i>b</i> [Å]	11.512(4)	18.575(13)	14.886(6)	13.685(5)
<i>c</i> [Å]	12.298(4)	12.637(7)	15.858(7)	12.770(4)
$\alpha$ [°]	69.890(6)	90	88.144(7)	90
$\beta$ [°]	80.995(6)	108.47(6)	73.229(7)	116.207(6)
$\gamma$ [°]	86.981(6)	90	69.927(7)	90
<i>V</i> [Å <sup>3</sup> ]	1215.1(7)	2330(2)	2620.0(19)	3508(2)
<i>Z</i>	2	4	2	8
<i>F</i> (000)	536	1028	1172	1600
<i>D</i> <sub>c</sub> [mgm <sup>-3</sup> ]	1.413	1.423	1.438	1.489
<i>T</i> [K]	293(2)	293(2)	293(2)	293(2)
$\theta$ range [°]	1.88–26.45	2.02–26.50	2.57–25.01	2.03–25.01
Goodness-of-fit on <i>F</i> <sup>2</sup>	1.019	1.084	1.015	1.000
<i>R</i> <sub>int</sub> [ <i>I</i> > 2σ( <i>I</i> )]	<i>R</i> <sub>1</sub> = 0.0494 <i>wR</i> <sub>2</sub> = 0.1069	<i>R</i> <sub>1</sub> = 0.0415 <i>wR</i> <sub>2</sub> = 0.1003	<i>R</i> <sub>1</sub> = 0.0799 <i>wR</i> <sub>2</sub> = 0.1812	<i>R</i> <sub>1</sub> = 0.0613 <i>wR</i> <sub>2</sub> = 0.1071

obtained free of charge from The Cambridge Crystallographic Data Centre via [www.ccdc.cam.ac.uk/data\\_request/cif](http://www.ccdc.cam.ac.uk/data_request/cif).

## Acknowledgments

This work was supported by the National Natural Science Foundation of China (20331010).

- [1] a) S. Noro, S. Kitagawa, M. Kondo, K. Seki, *Angew. Chem. Int. Ed.* **2000**, *39*, 2081–2084; b) M. Eddaoudi, J. Kim, N. L. Rosi, D. T. Vodak, J. Wachter, M. O’Keeffe, O. M. Yaghi, *Science* **2002**, *295*, 469–472; c) G. Férey, M. Latriche, C. Serre, F. Millange, T. Loiseau, A. Percheron-Guégan, *Chem. Commun.* **2003**, 2976–2977; d) L. Pan, M. B. Sander, X. Y. Huang, J. Li, M. Smith, E. Bittner, B. Bochrath, J. K. Johnson, *J. Am. Chem. Soc.* **2004**, *126*, 1308–1309.
- [2] a) K. S. Min, M. P. Suh, *Chem. Eur. J.* **2001**, *7*, 303–313; b) K. Uemura, S. Kitagawa, M. Kondo, K. Fukui, R. Kitaura, H. C. Chang, T. Mizutani, *Chem. Eur. J.* **2002**, *8*, 3587–3600; c) D. N. Dybtsev, H. Chun, S. H. Yoon, D. Kim, K. Kim, *J. Am. Chem. Soc.* **2004**, *126*, 32–33.
- [3] a) M. Albrecht, M. Lutz, A. L. Spek, G. van Koten, *Nature* **2000**, *406*, 970–974; b) L. G. Beauvais, M. P. Shores, J. R. Long, *J. Am. Chem. Soc.* **2000**, *122*, 2763–2772.
- [4] a) M. Fujita, Y. J. Kwon, S. Washizu, K. Ogura, *J. Am. Chem. Soc.* **1994**, *116*, 1151–1152; b) T. Sawaki, Y. Aoyama, *J. Am. Chem. Soc.* **1999**, *121*, 4793–4798; c) J. S. Seo, D. Whang, H. Lee, S. I. Jun, J. Oh, Y. Jeon, K. Kim, *Nature* **2000**, *404*, 982–986; d) L. Pan, H. M. Liu, X. G. Lei, X. Y. Huang, D. H. Olson, N. J. Turro, J. Li, *Angew. Chem. Int. Ed.* **2003**, *42*, 542–546.
- [5] a) H. L. Li, M. Eddaoudi, T. L. Groy, O. M. Yaghi, *J. Am. Chem. Soc.* **1998**, *120*, 8571–8572; b) K. S. Min, M. P. Suh, *J. Am. Chem. Soc.* **2000**, *122*, 6834–6840; c) R. Cao, D. F. Sun, Y. C. Liang, M. C. Hong, K. Tatsumi, Q. Shi, *Inorg. Chem.* **2002**, *41*, 2087–2094; d) C. D. Wu, C. Z. Lu, W. B. Yang, S. F. Lu, H. H. Zhuang, J. S. Huang, *Eur. J. Inorg. Chem.* **2002**, 797–800; e) Y. G. Li, N. Hao, Y. Lu, E. B. Wang, Z. H. Kang, C. W. Hu, *Inorg. Chem.* **2003**, *42*, 3119–3124; f) X. J. Zheng, L. P. Jin, S. Gao, *Inorg. Chem.* **2004**, *43*, 1600–1602.
- [6] a) T. M. Reineke, M. Eddaoudi, M. O’Keeffe, O. M. Yaghi, *Angew. Chem. Int. Ed.* **1999**, *38*, 2590–2594; b) M. Eddaoudi, H. Li, O. M. Yaghi, *J. Am. Chem. Soc.* **2000**, *122*, 1391–1397; c) D. T. Vodak, M. E. Braun, J. Kim, M. Eddaoudi, O. M. Yaghi, *Chem. Commun.* **2001**, 2534–2535; d) M. Eddaoudi, J. Kim, M. O’Keeffe, O. M. Yaghi, *J. Am. Chem. Soc.* **2002**, *124*, 376–377.
- [7] a) M. Kondo, T. Okubo, A. Asami, S. Noro, T. Yoshitomi, S. Kitagawa, T. Ishii, H. Matsuzaka, K. Seki, *Angew. Chem. Int. Ed.* **1999**, *38*, 140–143; b) D. F. Sun, R. Cao, Y. C. Liang, Q. Shi, W. P. Su, M. C. Hong, *J. Chem. Soc., Dalton Trans.* **2001**, 2335–2340; c) K. Barthelet, J. Marrot, D. Riou, G. Férey, *Angew. Chem. Int. Ed.* **2002**, *41*, 281–284; d) X. M. Zhang, M. L. Tong, M. L. Gong, X. M. Chen, *Eur. J. Inorg. Chem.* **2003**, 138–142.
- [8] a) M. Eddaoudi, D. B. Moler, H. Li, B. Chen, T. M. Reineke, M. O’Keeffe, O. M. Yaghi, *Acc. Chem. Res.* **2001**, *34*, 319–330; b) M. E. Braun, C. D. Steffek, J. Kim, P. G. Rasmussen, O. M. Yaghi, *Chem. Commun.* **2001**, 2532–2533; c) C. Ruiz-Pérez, P. Lorenzo-Luis, M. Hernández-Molina, M. M. Laz, F. S. Delgado, P. Gili, M. Julve, *Eur. J. Inorg. Chem.* **2004**, 3873–3879.
- [9] a) B. Q. Ma, P. Coppens, *Chem. Commun.* **2003**, 2290–2291; b) M. Liang, Q. L. Wang, L. H. Yu, D. Z. Liao, Z. H. Jiang, S. P. Yan, P. Cheng, *Polyhedron* **2004**, *23*, 2203–2208; c) E. Coronado, J. R. Galán-Mascarós, C. J. Gómez-García, E. Martínez-Ferrero, S. V. Smaalen, *Inorg. Chem.* **2004**, *43*, 4808–4810.
- [10] a) M. Oh, G. B. Carpenter, D. A. Sweigart, *Angew. Chem. Int. Ed.* **2003**, *42*, 2025–2028; b) F. A. A. Paz, J. Klinowski, *Inorg. Chem.* **2004**, *43*, 3882–3893.
- [11] a) J. Tao, M. L. Tong, X. M. Chen, *J. Chem. Soc., Dalton Trans.* **2000**, 3669–3674; b) S. A. Bourne, J. Lu, A. Mondal, B. Moulton, M. J. Zaworotko, *Angew. Chem. Int. Ed.* **2001**, *40*, 2111–2113; c) J. Sun, L. Weng, Y. Zhou, J. Chen, Z. Chen, Z. Liu, D. Zhao, *Angew. Chem. Int. Ed.* **2002**, *41*, 4471–4473; d) J. F. Ma, J. Yang, G. L. Zheng, L. Li, J. F. Liu, *Inorg. Chem.* **2003**, *42*, 7531–7534; e) D. N. Dybtsev, H. Chun, K. Kim, *Angew. Chem. Int. Ed.* **2004**, *43*, 5033–5036.
- [12] X. L. Wang, C. Qin, E. B. Wang, L. Xu, Z. M. Su, C. W. Hu, *Angew. Chem. Int. Ed.* **2004**, *43*, 5036–5040.
- [13] a) J. Tao, J. X. Shi, M. L. Tong, X. X. Zhang, X. M. Chen, *Inorg. Chem.* **2001**, *40*, 6328–6330; b) X. M. Chen, G. F. Liu, *Chem. Eur. J.* **2002**, *8*, 4811–4817; c) G. F. Liu, Z. P. Qiao, H. Z. Wang, X. M. Chen, G. Yang, *New J. Chem.* **2002**, *26*, 791–795; d) Y. Z. Zheng, G. F. Liu, B. H. Ye, X. M. Chen, *Z. Anorg. Allg. Chem.* **2004**, *630*, 296–300; e) Y. B. Wang, Z. M. Wang, C. H. Yan, L. P. Jin, *J. Mol. Struct.* **2004**, *692*, 177–186; f) M. Kondo, Y. Irie, Y. Shimizu, M. Miyazawa, H. Kawaguchi, A. Nakamura, T. Naito, K. Maeda, F. Uchida, *Inorg. Chem.* **2004**, *43*, 6139–6141.
- [14] E. Y. Choi, K. Park, C. M. Yang, H. Kim, J. H. Son, Y. H. Lee, D. Min, Y. U. Kwon, *Chem. Eur. J.* **2004**, *10*, 5535–5540.
- [15] F. A. A. Paz, Y. Z. Khimiyak, A. D. Bond, J. Rocha, J. Klinowski, *Eur. J. Inorg. Chem.* **2002**, 2823–2828.
- [16] S. R. Batten, B. F. Hoskins, B. Moubaraki, K. S. Murray, R. Robson, *Chem. Commun.* **2000**, 1095–1096.
- [17] a) J. W. Ko, K. S. Min, M. P. Suh, *Inorg. Chem.* **2002**, *41*, 2151–2157; b) H. Kumagai, C. J. Kepert, M. Kurmoo, *Inorg. Chem.* **2002**, *41*, 3410–3422.
- [18] V. Ramon, E. Albert, S. Xavier, F. B. Mercé, *Inorg. Chim. Acta* **1996**, *248*, 59–65.
- [19] G. M. Sheldrick, *SADABS, A Program for Empirical Absorption Correction of Area detector Data*, University of Göttingen, Germany, **1997**.
- [20] G. M. Sheldrick, *SHELXS 97, Program for Crystal Structure Solution*, University of Göttingen, Germany, **1997**.
- [21] G. M. Sheldrick, *SHELXL 97, Program for Crystal Structure Refinement*, University of Göttingen, Germany, **1997**.

Received: March 12, 2005

Published Online: September 5, 2005